Article

Terminalia ferdinandiana (Kakadu Plum)-Mediated Bio-Synthesized ZnO Nanoparticles for Enhancement of Anti-Lung Cancer and Anti-Inflammatory Activities

Zelika Mega Ramadhania [1,†], Jinnatun Nahar [1,†], Jong Chan Ahn [1], Dong Uk Yang [1], Jong Hak Kim [2], Dong Wook Lee [1], Byoung Man Kong [2], Ramya Mathiyalagan [1], Esrat Jahan Rupa [1], Reshmi Akter [1], Deok Chun Yang [1,2], Se Chan Kang [1,2,*] and Gi-Young Kwak [1,*]

1 Graduate School of Biotechnology, College of Life Sciences, Kyung Hee University, Yongin-si 17104, Korea; zelikamega@gmail.com (Z.M.R.); jinnatunnaharbph@gmail.com (J.N.); jongchanahn7@gmail.com (J.C.A.); rudckfeo23@naver.com (D.U.Y.); yu319@hanmail.net (D.W.L.); ramyabinfo@gmail.com (R.M.); eshratrupa91@gmail.com (E.J.R.); reshmiakterbph57@gmail.com (R.A.); dcyang@khu.ac.kr (D.C.Y.)

2 Department of Oriental Medicinal Biotechnology, College of Life Sciences, Kyung Hee University, Yongin-si 17104, Korea; jhkim@rgk.co.kr (J.H.K.); kong2167@naver.com (B.M.K.)

* Correspondence: sckang@khu.ac.kr (S.C.K.); kwakgiyoung8@gmail.com (G.-Y.K.)

† These authors contributed equally to this work.

Abstract: *Terminalia ferdinandiana* (Kakadu plum) is an Australian native plant that has recently gained the attention of researchers due to its highly antioxidant compounds that have substantial health benefits. To raise the value, in this study, it is used for the first time to synthesize ZnO nanoparticles for anti-lung cancer and anti-inflammatory activities. The formation of KKD-ZnO-NPs (ZnO particles obtained from Kakadu plum) were confirmed using a UV-Visible spectrophotometer. Fourier transform infrared (FTIR) spectroscopy analysis confirmed the functional groups that are responsible for the stabilization and capping of KKD-ZnO-NPs. The flower shape of the synthesized KKD-ZnO-NPs was confirmed by field emission-scanning electron microscopy (FE-SEM) and field emission-transmission electron microscopy (FE-TEM) analyses. The crystallites were highly pure and had an average size of 21.89 nm as measured by X-ray diffraction (XRD). The dynamic light scattering (DLS) revealed size range of polydisperse KKD-ZnO-NPs was 676.65 ± 47.23 nm with a PDI of 0.41 ± 0.0634. Furthermore, the potential cytotoxicity was investigated in vitro against human lung cancer cell lines (A549) and Raw 264.7 Murine macrophages cells as normal cells to ensure safety purposes using MTT assay. Thus, KKD-ZnO-NPs showed prominent cytotoxicity against human lung adenocarcinoma (A549) at 10 µg/mL and increased reactive oxygen species (ROS) production as well, which could promote toxicity to cancer cells. Moreover, upregulation of *p53* and downregulation of *bcl2* gene expression as apoptosis regulators were confirmed via RT-PCR. In addition, KKD-ZnO-NPs possess a similar capacity of reduction in proinflammatory-nitric oxide (NO) production when compared to the L-NMMA as inflammation's inhibitor, indicating anti-inflammatory potential. Incorporation of Kakadu plum extract as reducing and stabilizing agents enabled the green synthesis of flower-shaped KKD-ZnO-NPs that could be an initiative development of effective cancer therapy drug.

Keywords: anti-lung cancer; anti-inflammatory; green synthesis; Kakadu plum; zinc oxide nanoparticles

1. Introduction

Inflammation is an organism's defense mechanism against infectious environmental risk factors. It is also involved in the pathogenesis of a variety of human diseases, including the development and progression of cancer [1]. Cancer has become the leading cause

of death in humans; among the various cancers, lung cancer has the highest prevalence and the top of the deadliest cancer with an estimated 1.76 million mortality and 2.20 million new cases per year [2,3]. To date, a variety of conventional medications such as chemotherapies, radiation, and surgery have been used against cancer. These therapies are evidently effective in the destruction of cancer cells, but they exceed in the occurrence of adverse effects due to nonselective effects directed at normal cells as well. Due to the highly advanced nanomedicine, targeted drug delivery, and multi-target inhibitors, conventional therapies are gradually becoming obsolescent in cancer treatment [4]. Nanomedicine is a biomedical application of nanotechnology that employs nanoparticles (NPs) to treat diseases [5,6]. Several metal oxide nanoparticles are being developed to treat cancer. However, zinc oxide nanoparticles (ZnO-NPs) have markedly demonstrated their ability in the treatment of various kinds of cancer due to their bioactivity, biodegradability, and biocompatibility. Furthermore, ZnO-NPs exhibited specific toxicity against cancer cells via reactive oxygen species production and mitochondrial membrane potential destruction, resulting in cancer cell apoptosis [7]. In addition, ZnO-NPs have advantageous properties such as radiation adsorption, higher stability, electrochemical coupling coefficient, and non-toxic, inexpensive luminescent material that could enhance the performance of drug synthesis [8].

Physical and chemical methods have traditionally been used to create NPs. Green synthesis of NPs is becoming increasingly popular among researchers due to its significant interest in avoiding toxic chemicals, high costs, and harsh reaction conditions [9,10]. Bacteria, fungi, yeast, algae, and plants are among the biological sources used for the green synthesis of NPs. Plants have been identified as the best biological source for the synthesis of metal nanoparticles [11–13] due to their secondary metabolites, which can act as a natural reducing agent as well as a capping agent, and nanoparticles from plant materials are more stable than nanoparticles from other biological sources [14,15].

Terminalia ferdinandiana, known as Kakadu plum, belongs to the *Combretaceae* family, widely spread in northern and western Australia. The Kakadu plum is a yellowish-green fruit, 2.5 cm long and 1 cm in diameter, used traditionally as a refreshing drink in western Australia [16]. Phytochemical analysis has revealed that Kakadu plum is a rich source of vitamin C, flavonoid, and phenolic compounds [17,18]. As it is highly enriched in these compounds, Kakadu plum has numerous benefits on human health as an anticancer, antioxidant, liver protector, anti-inflammatory, and antibacterial agent [19–24]. Moreover, it is already reported that phenolic and flavonoid compounds could participate in Zn ions reduction and in the capping substance that stabilized ZnO-NPs [25–28].

While there is a great number of in-depth studies researched on cancer activities of Kakadu plum, the potential medicinal effects of Kakadu plum on lung cancer remain elusive. Notably, no previous research on the preparation of ZnO-NPs using Kakadu plum extract has been reported in the literature. Considering the advantages of Kakadu plum and ZnO, in this study, we carefully synthesized Kakadu plum-zinc oxide nanoparticles (KKD-ZnO-NPs) to investigate their cytotoxicity effect using the A549 lung cancer cell lines and Raw 264.7 as non-cancerous cells. Furthermore, the anticancer activity was assessed by measuring the level of ROS and gene expression of apoptosis regulators such as *p53* (tumor suppressor protein), and *bcl2* was observed by RT-PCR. In addition, to determine the anti-inflammatory effect of KKD-ZnO-NPs on the LPS-induced proinflammatory reaction, such as nitric oxide (NO), the production level of NO was determined using Griess reagent.

2. Materials and Methods

2.1. Materials and Chemicals

The Kakadu plum sample was provided by KAKADU LIFE (Canning Vale, Australia) from Northern Territory as dried fruits. The dried Kakadu plum fruits were ground into moderately fine powder to optimize the extraction process. Zinc nitrate hexahydrate

($Zn(NO_3)_2 \cdot 6H_2O$; >98.0%) (Sigma-Aldrich, Saint Louis, MI, USA), sodium hydroxide (>98.0%), absolute alcohol was supplied by Samchun Pure Chemical Co. Ltd. (Gyeonggi-do, South Korea). The lung cancer cell line (A549) and Raw 264.7 murine macrophage cells used in this study were obtained from the Korean Cell Line Bank (KCLB, South Korea). Roswell Park Memorial Institute (RPMI) 1640, Dulbecco's Modified Eagle Medium (DMEM) culture medium was purchased from Welgene Inc. (South Korea) with 10% fetal bovine serum (FBS) and 1% penicillin/streptomycin (p/s) (Welgene Inc., Gyeongsan-si, South Korea) was also used for experiments.

2.2. Preparation of Kakadu Plum Extract

In order to obtain the extracts, reflux was chosen for the extraction method. Initially, 2 g of sample powder was extracted with 40 mL of water. Extraction was performed at 95 degrees for 2 h with three processing times. In every processing time, the mixture was filtered, collected, and evaporated to remove the solvent using a rotary evaporator. The prepared extract was stored at 4 °C for further use [24].

2.3. Green Synthesis of KKD-ZnO-NPs

Kakadu plum-zinc oxide nanoparticles (KKD-ZnO-NPs) were synthesized using co-precipitation with minor modifications [12]. Initially, 1 mL of Kakadu plum extract (40 mg/mL, *w/v*) was mixed with 100 mL of distilled water under stirring, and 0.1 mM (10 mL) of $Zn(NO3)_2 \cdot 6H_2O$ solution was added to the mixed solution and was heated up to 70 °C. NaOH 0.2 M (15 mL) was added dropwise to the mixture, and the solution was kept over the hot plate for at least 2 h with a continuous stirrer at 500 rpm. The color changes of the solution to milky white indicate the formation of KKD-ZnO-NPs. After the completed precipitation of nanoparticles, the suspension was centrifuged for 15 mins at 5000 rpm. The KKD-ZnO-NPs were washed twice and purified by centrifugation. Furthermore, we kept it in a 60 °C dryer for 4 h for a complete formation of $Zn(OH)_2$ to ZnO-NPs as a white KKD-ZnO-NPs powder.

2.4. Characterization of KKD-ZnO-NPs

The KKD-ZnO-NPs were first examined using ultraviolet-Visible (UV-Vis) spectroscopy in the 200–700 nm range on an Ultraspec™ 2100 pro with a 10 mm path length quartz cuvette (2100 Pro, Amersham Biosciences Corp., Piscataway, NJ, USA). The FTIR spectra were obtained using a PerkinElmer Spectrum 100 spectrometer (PerkinElmer Inc., Waltham, MA, USA). KKD-ZnO-NPs powders were scanned in the range 4000–450 cm^{-1} at a resolution of 4 cm^{-1} on KBr pellets. The size distribution and zeta potential of KKD-ZnO-NPs in water data were determined on particle size analyzer ELS-Z2 series (Otsuka Electronics Cp. Ltd., Osaka, Japan) at 25 °C. A JEM-2100F was used to capture the images of field emission-transmission electron microscopy (FE-TEM) (JEOL, Akishima, Tokyo, Japan). A few drops of sample were placed on a carbon grid and dried at 60 °C. To obtain topographical and elemental mapping we used a field emission-scanning electron microscopy (FE-SEM) by LEO SUPRA 55, GENESIS 200 (Carl Zeiss, Jena, Germany); gun: thermal field emission type; resolution: 1.0 nm @15 kV 1.7 nm @ 1 kV 4.0 nm @ 0.1 kV; magnification: 12× to 900,000×). The XRD analyzer was performed on an energy-dispersive X-ray spectrophotometer (D8 Advance, Hannover, Germany), operated at 40 kV, 40 mA, with a CuKα radiation of 1.54 Å, over the 2θ range of 10–80° at 6 min with a sampling interval of 0.02 in room temperature. The crystal size diameter could be calculated using the Scherrer equation:

$$D = \frac{0.9\lambda}{\beta \cos\theta} \tag{1}$$

In this equation, D denotes the crystalline size in nanometers (nm), λ is the X-ray wavelength of CuKα radiation in nm, the full width at half maximum (FWHM) is in radians, and θ is the half of the Bragg angle in radians.

2.5. Cell Culture

Human lung carcinoma (A549) was developed in 89% RPMI 1640 growth media with 10% FBS and 1% penicillin-streptomycin. Generally, murine macrophage (RAW 264.7) cells were refined in DMEM with 10% FBS and 1% penicillin-streptomycin. Two cell lines were incubated at 5% CO_2 atmosphere in a 37 °C humidified incubator and were permitted to adhere and grow for 24 h prior to treatment with different samples.

2.6. In Vitro Cytotoxicity of Kakadu Plum Extract and KKD-Zn-NPs

The cytotoxicity of the Kakadu extract and Kakadu-ZnO-NPs were analyzed on A549 and RAW 264.7 cell lines using MTT solution. Only A549 cells were used to test the cytotoxicity of cisplatin (10 μg/mL), and the results were compared to KKD-ZnO-NPs after 24 h. Cell viability test was proceeded as previously discussed [12]. First, cancer cells and normal cells were plated at a selective density of 1×10^4 cells/well in a 96-well plate. Then Cells were medicated with several concentrations (0, 2.5, 5, 10, 20 μg/mL) and incubated for 24 h. After 24 h, cells were treated with 20 μL of 3-(4, 5-dimethyl-2-thiazolyl)-2, 5-diphenyl tetrazolium bromide solution (MTT; 5 mg/mL, in PBS; Life Technologies, Eugene, OR, USA) for 3–4 h at 37 °C. Moreover, for viable cells, purple-colored formazan is formed by adding MTT reagents. In each well, 100 μL of DMSO was added for dissolving the insoluble formazan agents. The results were obtained using an Enzyme-Linked Immunosorbent Assay (ELISA) reader at 570 nm (Bio-Tek, Instruments, Inc., Winooski, VT, USA).

2.7. Reactive Oxygen Species (ROS) Generation Assay

We detected the reactive oxygen species (ROS) intensity by 2′,7′-dichlorodihydro-fluorescein diacetate (DCFH-DA) on Human lung carcinoma (A549). We seeded the cells at a specific density of 1×10^4 per well to allow attachment in 96-well cell culture plates and kept them in the incubator overnight for 100% growth confluency. Next, A549 cells were treated with different concentrations of cisplatin (10 μg/mL), KKD-Ext, and KKD-ZnO-NPs (0, 2.5, 5, and 10 μg/mL) for 24 h. After 24 h treatment periods, the cell was stained with 100 μL of DCFH-DA (10 μM) solution into each well and incubated for 30 min in dark condition. Then old media were discarded, and cells were washed twice with PBS (100μL/well). A multi-model plate reader (spectrofluorometer) was used for determination of the fluorescence intensity of ROS generation at an excitation wavelength of 485 nm and an emission wavelength of 528 nm. The increase in ROS was probed by DCFH-DA reagent.

2.8. Reverse Transcription Polymerase Chain Reaction (RT-PCR)

Total RNA from A549 cells was isolated with QIAzol lysis reagent (QIAGEN, Germantown, MD, USA), and the reverse transcription reaction was performed by using 1 μg of RNA in 20 μL of reaction buffer of amfiRivert reverse transcription reagents (GenDepot, Barker, TX, USA) as described by the manufacturer's instruction. The obtained cDNA was amplified with the following primers: *bcl2*, forward 5′-GAA GGG CAG CCG TTA GGA AA-3′ and reverse 5′-GCG CCC AAT ACG ACC AAA TC-3′; *p53*, forward 5′-TCT TGG GCC TGT GTT ATC TCC-3′ and reverse 5′-CGC CCA TGC AGG AAC TGT TA-3′; GAPDH, forward 5′-CAA GGT CAT CCA TGA CAA CTT TG-3′ and reverse 5′-GTC CAC CAC CCT GTT GCT GTA G-3′. The reaction was cycled 35 times, for 30 s at 95 °C, 30 s at 60 °C, and 50 s at 72 °C. Using 1% agarose gels, the amplified RT-PCR products were analyzed, visualized by *Safe-Pinky* DNA Gel Staining (GenDepot, Barker, TX, USA), and captured under ultraviolet light.

2.9. Measurement of Nitrite Levels

The measurement of nitric oxide (NO) level was described previously [29]. RAW 264.7 cells (1×10^4 cells/well) were plated into 24-well culture plates and kept in the incubator at 37 °C in a humidified condition containing 5% CO_2 for 24 h. Then cells were pretreated with various concentrations of KKD-Ext and KKD-ZnO-NPs samples for 1 h. After treatment, 1 μg/mL lipopolysaccharide (LPS) was added as a stimulator (to induce and cause inflammation) in the presence of samples and kept incubated for 1 day. Griess reagent was used to determine the nitrite levels in the cell medium. In summary, an equivalent volume of Griess reagent was combined with 100 μL of stimulated supernatant. The resulting absorbance at 540 nm was measured against the standard curve generated with sodium nitrite using a microplate reader (Bio-Tek, Instruments, Inc., Winooski, VT, USA). In this experiment, L-NMMA was used as a standard inhibitor (positive control) at a concentration of 50 μM. Every assay was performed three times, and the data were expressed as NO production (%).

3. Results and Discussion

3.1. UV-Visible Spectroscopy

The co-precipitation method was used to create KKD-ZnO-NPs, and after completely adding NaOH, the resulting mixture gradually turned milky in color. The resulting KKD-ZnO-NPs were tested using a UV-Visible spectrophotometer after purification and drying at 60 °C for 4 h.

Figure 1 shows the UV-Visible absorption spectrum of KKD-ZnO-NPs. At 362 nm, the maximum absorbance peak, also known as the maximum surface plasmon resonance (SPR) peak, corresponds to the surface plasmon of oscillating electron of KKD-Zn-NPs, resulting in strong light extinction. The absorbance peak of ZnO nanoparticles is reported to be between 310 and 365 nm in wavelength [30]. On the other contrary, the SPR peak was not present in the absorbance spectra of Kakadu plum extract. As many reported that Kakadu plum extract contains a high amount of polyphenolic derivates, such as flavonoids and phenolic acids [31,32], the polyphenol peak contained in Kakadu plum extract was expected to be observed around 280–320 nm [33]. The polyphenol compound acts as a reducing agent, donating electrons to metal ions and converting them to NPs. These NPs occur in a high-surface-energy state and strive to aggregate with one another in order to convert to their low-surface-energy conformations. As a result, the existence of more reducing and stabilizing agents inhibits nanoparticle aggregation and enables the production of smaller NPs [34].
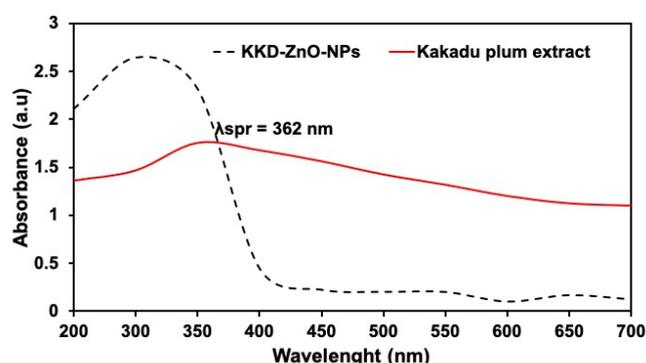

Figure 1. Visible spectra of KKD-ZnO-NPs with Kakadu plum extract.

3.2. FTIR Analysis

FTIR analysis assisted in identifying functional groups present in plant extracts that contribute to the mechanism of bonding with Zn-O NPs. Figure 2 shows the FTIR spectra of KKD-Zn-NPs, which were acquired in the range 400–4000 cm^{-1} using the KBr method.

The broad peak at 3289.80 cm⁻¹ resulted from the O-H stretching of Kakadu plum adsorbed phenolic compounds on the surface of KKD-ZnO-NPs. Due to the complexation of functional groups present in Kakadu plum and the surface of KKD-ZnO-NPs, some transmitted peaks that appeared at 2910 and 1710 cm⁻¹ of KKD-ZnO-NPs exhibited shifts to lower wavenumber. Because of the asymmetric and symmetric stretching of C-H and C=O (ketones) bonds, these peaks were associated with the presence of aromatic compounds. Transmission peaks observed at 1320 cm⁻¹ were proposed to be contributed by the stretching of C-O bonds of carbonyl groups and/or C-O of alcoholic groups and glycosidic linkages of the phytochemical constituents of Kakadu plum. Finally, there was a strong transmission peak that appeared around 500 cm⁻¹ is correlated to Zn-O [35–39].
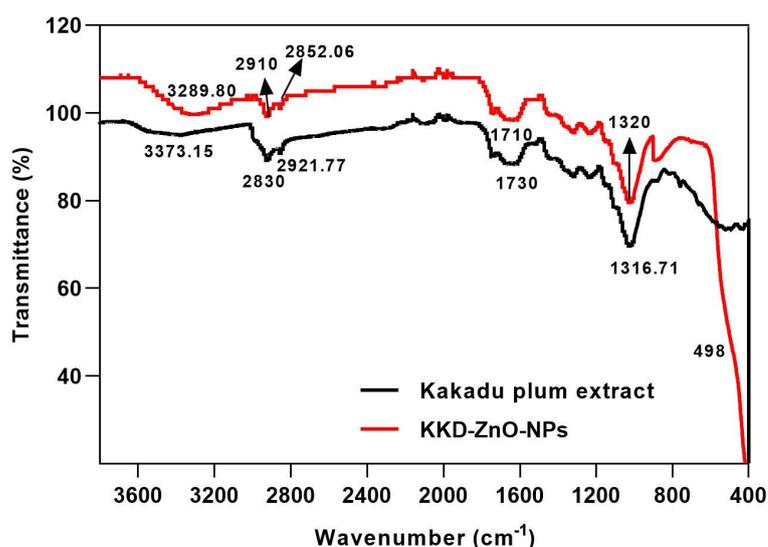

Figure 2. FTIR spectrum of KKD-ZnO-NPs (red) and Kakadu plum extract (black).

3.3. Particle Size Distribution Analysis

The dynamic light scattering (DLS) method was used to analyze the particle size distribution of KKD-ZnO-NPs. According to DLS analysis, the hydrodynamic Z-average of KKD-ZnO-NPs was 676.65 ± 47.23 nm with a PDI of 0.41 ± 0.0634 (Figure 3). In the following discussion, the obtained hydrodynamic size was in accordance with the particle size range observed by FE-TEM (500–1000 nm). A zeta analyzer was used to test the nanoparticle's stability; the KKD-ZnO-NPs zeta potential observed was around −23.75 ± 0.2 mV, confirming the nanoparticle's stability. The low PDI value indicated that nano composition was polydisperse with multiple size populations, which was confirmed by FE-TEM and FE-SEM.
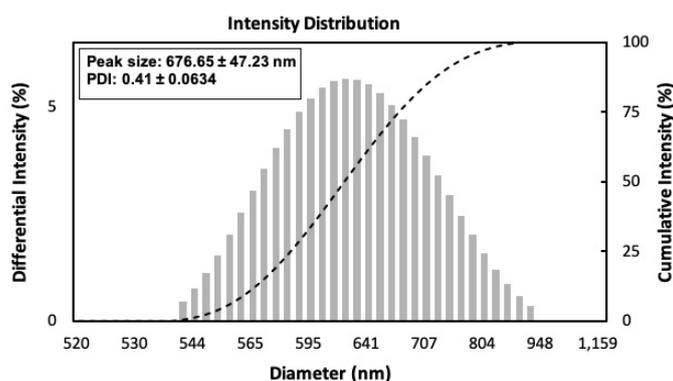

Figure 3. Dynamic light scattering (DLS) indicating size distribution of KKD-ZnO-NPs.

3.4. FE-TEM and FE-SEM Analysis

FE-TEM was used to examine the structure of the KKD-ZnO-NPs. As shown in Figure 4A–C, KKD-ZnO-NPs exhibited flower shapes with sizes ranging from 500 to 1000 nm. The formation of these nanoflowers was believed to be caused by the aggregation of smaller polygonal ZnO-NPs, resulting in ZnO nanoflowers with 4–6 broad arrow petal-like structures. The element mapping results revealed the distribution of zinc and oxygen in the nanoflowers, which were represented as red and green dots, respectively (Figure 4D). The hexagonal rings of electron spots in KKD-ZnO-NPs SAED patterns correspond to each facet of the sample's lattice planes, indicating the KKD-ZnO-NPs highly crystalline structure (Figure 4E) [40,41]. The EDX spectra revealed the highest optical peaks measured with 83.82% weight of zinc and 16.15% weight of oxygen, making it 100%, confirming the purity of KKD-ZnO-NPs (Figure 4F).
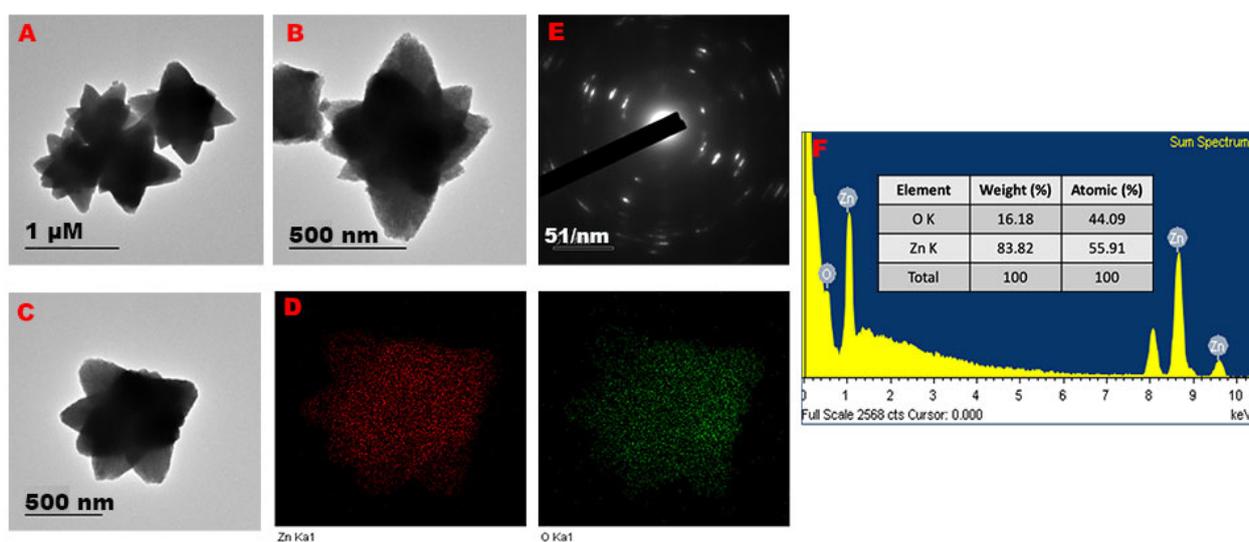

Figure 4. FE-TEM images of KKD-ZnO-NPs showing the structure of particles (**A–C**), elemental distribution (**D**), zinc (red) and oxygen (green), selected area electron diffraction (SAED) (**E**), energy-dispersive X-ray spectroscopy (EDX) spectrum (**F**).

The FE-SEM analysis confirmed that the KKD-ZnO-NPs exhibited a flower-shaped morphology, which is consistent with the FE-TEM data (Figure 5A,B). These findings showed similarly shaped ZnO-NPs are prepared using plant extract and bacteria, as reported earlier [42,43]. A sharp peak signal of both metals in the EDX spectra indicated the presence of Zn and O, reveals the presence of metal oxide nanoparticles, and verifying the absence of aggregation, agreed with other references [44,45].
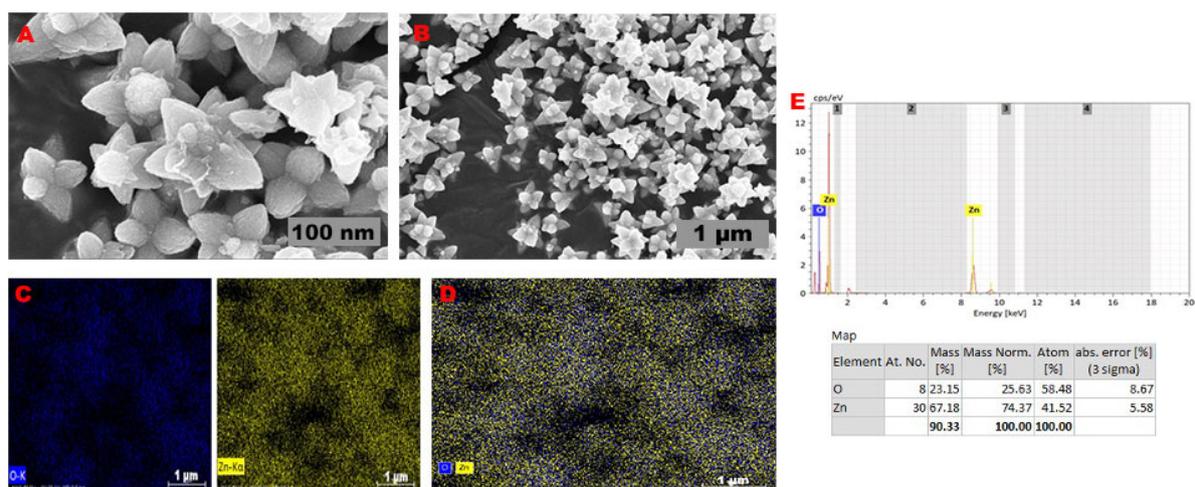
Figure 5. FE-SEM images of KKD-ZnO-NPs exhibited a flower shape in (**A**), (**B**), elemental distribution (**C**,**D**), zinc (yellow) and oxygen (blue), and EDX quantitative analysis (**E**).

3.5. X-ray Diffraction (XRD)

The formation of biosynthesized KKD-ZnO-NPs was confirmed by X-ray diffraction measurements (Figure 6). The diffraction peaks appeared at 2θ value of 31.830°, 34,451°, 36.316°, 47.578°, 56.634°, 62.945°, and 68.023° corresponding to (100), (002), (101), (102), (110), (103), and (112) crystal planes, respectively. The most intense peak at 36.316° belongs to the (101) orientation, and its position reflects the hexagonal wurtzite structure in the sample [46].
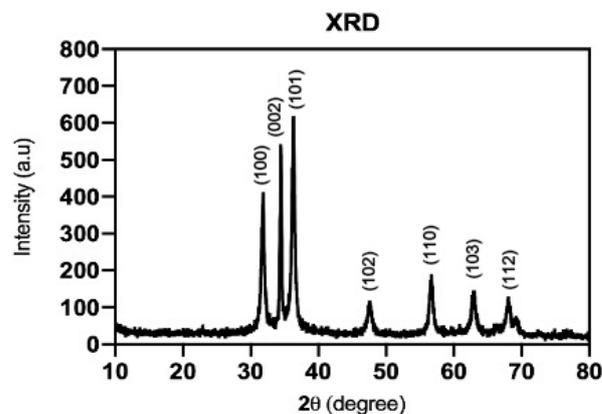

Figure 6. XRD pattern of KKD-ZnO-NPs.

The Scherrer equation was used to calculate the average crystallite diameter of KKD-ZnO-NPs by taking the crystallite sizes of the three most intense peaks, namely (100), (002), and (101) in accordance with literature and JCPDS data [47–49], as shown in Table 1.

Table 1. XRD analysis of the crystalline size of KKD-ZnO-NPs.

Lattice Plane	Position of Peak (2θ)	D Spacing Value (A°)	FWHM Value (2θ)	Size (nm)	Average (nm)
100	31.830	2.80915	0.4905	16.85	
002	34.451	2.60116	0.2747	30.30	21.89
101	36.316	2.47176	0.4513	18.54	
102	47.578	1.90966	1.025	8.48	

110	56.634	1.6239	0.7457	12.11
103	62.945	1.47543	0.9419	9.88
112	68.023	1.3771	0.8438	11.37

3.6. Cytotoxicity Effect of Kakadu Plum Extract and KKD-ZnO-NPs

According to our findings, we observed the cytotoxicity level of the Kakadu plum extract and KKD-ZnO-NPs on murine macrophage (RAW 264.7) cells and A549 lung cancer cells were medicated several concentrations (0, 2.5, 5, 10, 20 µg/mL) for 24 h. In the cytotoxicity experiment, we used MTT solution for measuring the cell toxic level. Evaluation of the cytotoxicity in cancer-free RAW 264.7 cells was determined as safety of samples. It was observed that cell viability of RAW 264.7 cells was showed low toxicity with Kakadu plum extract and KKD-ZnO-NPs at 20 µg/mL after 24 h (Figure 7A).
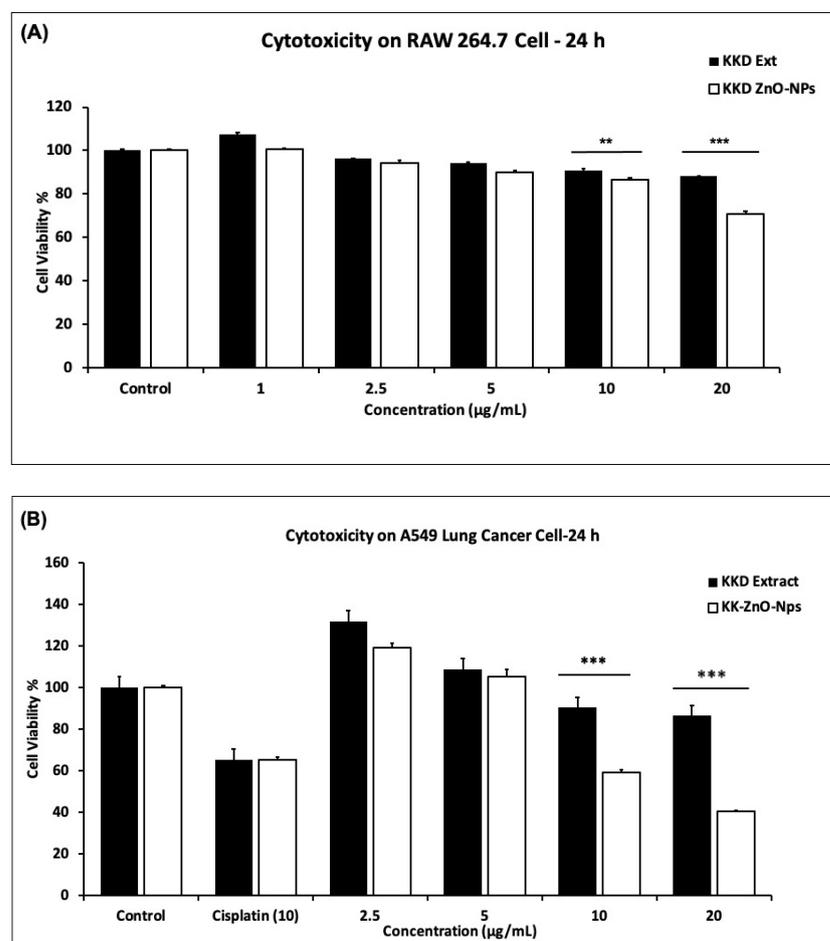

Figure 7. In vitro, cell cytotoxicity evaluation for Kakadu plum extract and KKD-ZnO-NPs (**A**) on murine macrophage (RAW 264.7), (**B**) on human lung carcinoma (A549) cells compared to positive control (cisplatin). Graph shows mean ± SD values of four replicates. ** $p < 0.01$; *** $p < 0.001$ indicates significant differences from control groups.

On the other hand, it was observed that KKD-ZnO-NPs decreased A549 cell viability in a dose-dependent manner. Additionally, cytotoxicity determination was performed for KKD-ZnO-NPs compared to positive control such as commercial cisplatin, which is used as an anticancer drug. Results observed in Figure 7B, at the concentration of 10 µg/mL, KKD-ZnO-NPs had much higher toxicity than cisplatin. This study's cytotoxicity results are consistent with a previous report that observed *Mangifera indica* leaves mediated ZnO-NPs, which could enhance the anticancer activity [50]. Moreover, there were several pieces of literature that reported the anticancer activity of ZnO nanoparticles [4,9,51,52]. ZnO

nanoparticles have the ability to dissolve Zn ions in the extracellular region by themselves, which in turn leads to increased intracellular Zn^{2+} levels. ZnO-NPs are able to penetrate easily through the cell membrane to damage the mitochondrial and specific DNA sequences so that the medication significantly represses the growth of the tumor with the specific target location and specific cytotoxicity. Past examination detailed the anticancer impact of ZnO-NPs in cancer cells [53,54]. Not only as reducing and stabilizing agents, but Kakadu plum extract could also enhance the anticancer effect on human lung cancer cell line (A549). Hence, the current investigation suggests that at a limit dosage (10 μg/mL), KKD-ZnO-NPs are effective as a cancer therapy drug with minimum toxicity.

3.7. In Vitro ROS Induced by KKD-ZnO-NPs

Intracellular ROS level was determined by the DCFH-DA reagent with cisplatin, Kakadu plum extract, and KKD-ZnO-NPs on A549 cells. Zinc oxide nanoparticles (ZnO-NPs) are important reputed materials for anticancer activity due to reactive oxygen species (ROS) generation [55]. However, KKD-ZnO nanoparticles have not been reported on anticancer activity. In our study, we focused on the preparation of KKD-ZnO-NPs and their application in human lung carcinoma (A549). For evaluation of intracellular ROS production, cells were medicated with cisplatin, Kakadu plum extract, and KKD-ZnO-NPs for 24 h with different concentrations. The DCFH-DA reagent was used to test the expansion of ROS levels. As displayed in Figure 8, KKD-ZnO-NPs created a higher ROS level compared to Kakadu extract at 10 μg/mL. Additionally, ZnO nanoparticles initiate oxidative stress in cancer cells, one of the top mechanisms that have the ideal capability on cytotoxicity examination [56–58]. Generally, the cell cytotoxicity was observable due to insoluble criteria of ZnO nanoparticles to free Zn^{2+} (higher concentration). The properties of ZnO-NPs can induce ROS at the body surface, resulting in cell death when the ROS ratio exceeds the antioxidant level of the cell [59]. These findings suggest that KKD-ZnO-NPs might be a potential anticancer drug treating lung cancer.
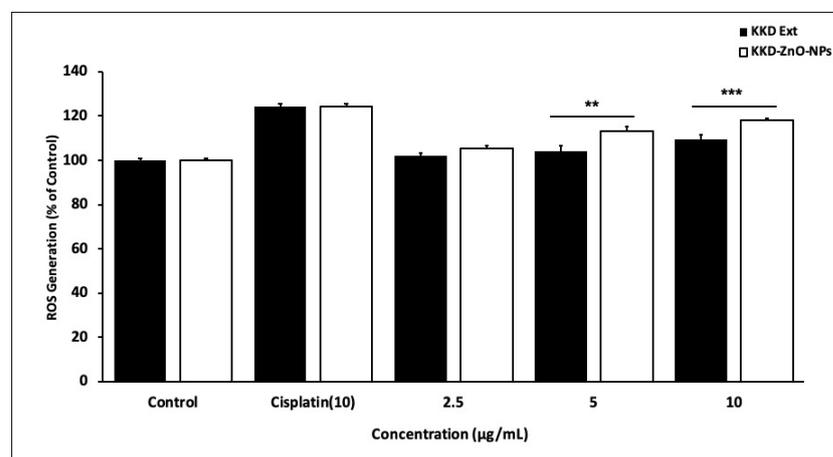

Figure 8. In A549 cells, the ability of KKD-Ext, and KKD-ZnO-NPs to generate intercellular reactive oxygen species (ROS) was compared to a positive control (cisplatin). Graph shows mean ± SD values of three replicates. ** $p < 0.05$; *** $p < 0.001$ indicates significant differences from control groups.

3.8. Effect of KKD-ZnO-NPs on Gene Expression of Apoptosis Regulator

The production of ROS by cells is essential for redox signaling, while *p53* (tumor suppressor protein) is a redox active transcription factor. ROS can activate *p53* and mediates apoptosis on cancer cells [60,61]. *p53* regulates the expression of several microRNA species, including miR-34, which is known to target the pro-survival *bcl2* gene. *bcl2* regulated pathway is one of the apoptosis pathways that is activated by stress conditions such as cytokine deprivation or DNA damage [62].

The RT-PCR (Figure 9) showed upregulation of *p53* and downregulation of *bcl2* gene expression in a dose-dependent manner by KKD-ZnO-NPs compared to Kakadu plum extract only. This phenomenon may be due to the activation of mitochondrial-mediated apoptosis, which is characterized by the downregulation of *bcl2*, followed by an increase in Bax, allowing cytochrome C release into the cytosol, and finally, the caspase 9/3 signaling cascade [63,64]. However, quantitative analysis and further investigation of the molecular mechanisms are needed to clarify the cellular pathways.
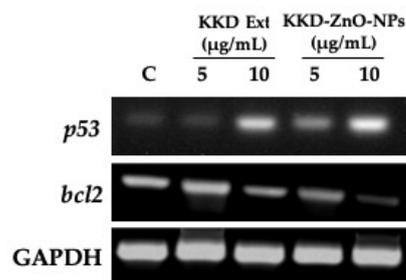

Figure 9. RNA expression of apoptosis pathway genes after treatment of KKD-Ext and KKD-Zn-NPs on A549 cells (24 h).

3.9. Effect of KKD-ZnO-NPs on NO Production in LPS-Activated RAW 264.7 Cells

Macrophages generate nitric oxide (NO) as a primary mediator during inflammation reactions. It is made from the amino acid arginine by the enzyme inducible nitric oxide synthase (iNOS) [29]. NO production is required for a variety of physiological tasks, such as a neurotransmitter and influencing blood flow and synaptic plasticity. In contrast, overexpression of NO production in macrophages can able to abolish and induce dysfunction along with normal cells [65]. NO is a major mediator that is important in the progression of inflammation. As a result, a medication that suppresses NO formation is also recognized as a therapeutic agent for inflammation and cancer management.

The inhibitory effect of Kakadu plum extract and KKD-ZnO-NPs on LPS-stimulated NO production in RAW264.7 cells were measured using the Griess reagents. At the concentration of 10 µg/mL, Kakadu plum extract and KKD-ZnO-NPs were able to suppress the NO production in LPS-stimulated RAW 264.7 cells by 29.28% and 41.46%, respectively, against the LPS-treated group (Figure 10). The standard NO inhibitor, L-NMMA, which was used as a positive control in this work, greatly decreased NO production level. Therefore, KKD-ZnO-NPs can decrease the release of NO level, indicating its anti-inflammatory potential.
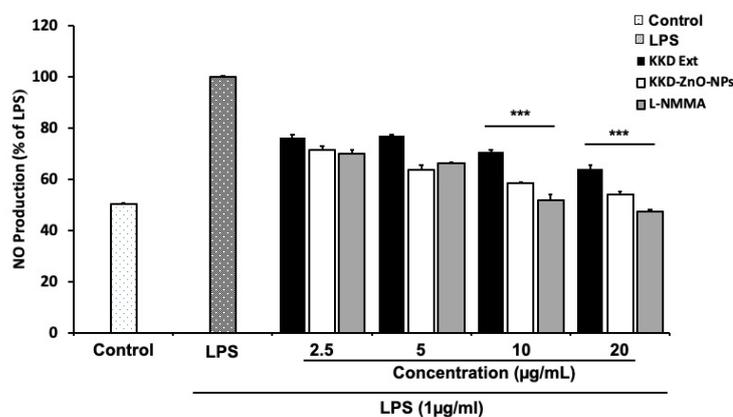

Figure 10. Effects of Kakadu plum extract (KKD-Ext) and KKD-ZnO-NPs on NO production. Control (non-treated cells). LPS (1 µg/mL)-treated RAW cells (to induce NO production and cause inflammation). Graph shows mean ± SD values of three replicates. *** $p < 0.001$ as compared to the group treated with LPS alone.

4. Conclusions

Incorporation of Kakadu plum extract as reducing and stabilizing agents enabled the green synthesis of flower-shaped KKD-ZnO-NPs. The UV-Vis, FTIR, XRD, DLS, TEM, and SEM structural and optical analysis confirmed the formation of efficient KKD-ZnO-NPs. In vitro cytotoxicity testing revealed that KKD-ZnO-NPs had anticancer efficacy on human lung cancer cell lines (A549) as well as the production of ROS. On human lung carcinoma cells, KKD-ZnO-NPs induced higher ROS levels than Kakadu plum extract only. Moreover, KKD-ZnO-NPs upregulated *p53* and suppressed *bcl2* gene expression as regulators of cancer cell apoptosis. On the other hand, chronic or recurrent acute inflammation caused by infectious agents or other sources has the potential to promote tumor formation, growth, emergence, and malignant transformation. Furthermore, cancer and inflammatory tissues offer a number of vascular mediators, including NO, and their most notable physiological effect is increased vascular permeability. Moreover, our results showed that KKD-ZnO-NPs possess a similar capacity of reducing NO production compared to the L-NMMA as positive control. Based on the enhanced permeability and retention (EPR) effect of macromolecular drugs, enhanced vascular permeability of tumor and inflammatory tissue is the key to future drug development of highly specific targeting of the desired tumors or inflammatory lesions. However, further biological studies are needed to characterize the molecular mechanisms of KKD-ZnO-NPs and to clarify the cellular pathways involved. This approach may be an effective cancer treatment that breaks the link between inflammation and cancer. Taken together, our findings suggest that KKD-ZnO-NPs at limited dosage (10 μg/mL) could be a promising candidate for the development of a pharmaceutically effective cancer therapy drug with minimum toxicity.

References

1.　Suh, S.-S.; Hong, J.-M.; Kim, E.J.; Jung, S.W.; Kim, S.-M.; Kim, J.E.; Kim, I.-C.; Kim, S. Anti-inflammation and Anti-Cancer Activity of Ethanol Extract of Antarctic Freshwater Microalga, *Micractinium* sp. *Int. J. Med. Sci.* **2018**, *15*, 929.

2.　Thai, A.A.; Solomon, B.; Sequist, L.V.; Gainor, J.F.; Heist, R.S. Lung Cancer. *Lancet* **2021**, *398*, 535–554.

3.　Sung, H.; Ferlay, J.; Siegel, R.L.; Laversanne, M.; Soerjomataram, I.; Jemal, A.; Bray, F. Global cancer statistics 2020: GLOBOCAN estimates of incidence and mortality worldwide for 36 cancers in 185 countries. *CA Cancer J. Clin.* **2021**, *71*, 209–249.

4.　Bisht, G.; Rayamajhi, S. ZnO nanoparticles: A promising anticancer agent. *Nanobiomedicine* **2016**, *3*, 3–9.

5.　Wang, R.; Billone, P.S.; Mullett, W.M. Nanomedicine in action: An overview of cancer nanomedicine on the market and in clinical trials. *J. Nanomater.* **2013**, *2013*, 8–10.

6.　Sharifi-Rad, J.; Quispe, C.; Butnariu, M.; Rotariu, L.S.; Sytar, O.; Sestito, S.; Rapposelli, S.; Akram, M.; Iqbal, M.; Krishna, A. Chitosan nanoparticles as a promising tool in nanomedicine with particular emphasis on oncological treatment. *Cancer Cell Int.* **2021**, *21*, 1–21.

7.　Anjum, S.; Hashim, M.; Malik, S.A.; Khan, M.; Lorenzo, J.M.; Abbasi, B.H.; Hano, C. Recent Advances in Zinc Oxide Nanoparticles (ZnO NPs) for Cancer Diagnosis, Target Drug Delivery, and Treatment. *Cancers* **2021**, *13*, 4570.

8.　Özgür, Ü.; Alivov, Y.I.; Liu, C.; Teke, A.; Reshchikov, M.; Doğan, S.; Avrutin, V.; Cho, S.-J.; Morkoç, H. A comprehensive review of ZnO materials and devices. *J. Appl. Phys.* **2005**, *98*, 11.

9. Umamaheswari, A.; Prabu, S.L.; John, S.A.; Puratchikody, A. Green synthesis of zinc oxide nanoparticles using leaf extracts of *Raphanus sativus* var. Longipinnatus and evaluation of their anticancer property in A549 cell lines. *Biotechnol. Rep.* **2021**, *29*, e00595.

10. Shreyash, N.; Bajpai, S.; Khan, M.A.; Vijay, Y.; Tiwary, S.K.; Sonker, M. Green synthesis of nanoparticles and their biomedical applications: A review. *ACS Appl. Nano Mater.* **2021**, *4*, 11428–11457.

11. Geetha, R.; Ashokkumar, T.; Tamilselvan, S.; Govindaraju, K.; Sadiq, M.; Singaravelu, G. Green synthesis of gold nanoparticles and their anticancer activity. *Cancer Nanotechnol.* **2013**, *4*, 91–98.

12. Rupa, E.J.; Arunkumar, L.; Han, Y.; Kang, J.P.; Ahn, J.C.; Jung, S.-K.; Kim, M.; Kim, J.Y.; Yang, D.-C.; Lee, G.J. *Dendropanax morbifera* extract-mediated ZnO nanoparticles loaded with indole-3-carbinol for enhancement of anticancer efficacy in the A549 human lung carcinoma cell line. *Materials* **2020**, *13*, 3197.

13. El Shafey, A.M. Green synthesis of metal and metal oxide nanoparticles from plant leaf extracts and their applications: A review. *Green Process. Synth.* **2020**, *9*, 304–339.

14. Jain, N.; Jain, P.; Rajput, D.; Patil, U.K. Green synthesized plant-based silver nanoparticles: Therapeutic prospective for anticancer and antiviral activity. *Micro. Nano. Syst. Lett.* **2021**, *9*, 1–24.

15. Erdogan, O.; Abbak, M.; Demirbolat, G.M.; Birtekocak, F.; Aksel, M.; Pasa, S.; Cevik, O. Green synthesis of silver nanoparticles via *Cynara scolymus* leaf extracts: The characterization, anticancer potential with photodynamic therapy in MCF7 cells. *PLoS ONE* **2019**, *14*, e0216496.

16. Konczak, I.; Roulle, P. Nutritional properties of commercially grown native Australian fruits: Lipophilic antioxidants and minerals. *Food Res. Int.* **2011**, *44*, 2339–2344.

17. Konczak, I.; Zabaras, D.; Dunstan, M.; Aguas, P. Antioxidant capacity and hydrophilic phytochemicals in commercially grown native Australian fruits. *Food Chem.* **2010**, *123*, 1048–1054.

18. Konczak, I.; Maillot, F.; Dalar, A. Phytochemical divergence in 45 accessions of *Terminalia ferdinandiana* (Kakadu plum). *Food Chem.* **2014**, *151*, 248–256.

19. Tan, A.C.; Konczak, I.; Ramzan, I.; Zabaras, D.; Sze, D.M.-Y. Potential antioxidant, antiinflammatory, and proapoptotic anticancer activities of Kakadu plum and Illawarra plum polyphenolic fractions. *Nutr. Cancer* **2011**, *63*, 1074–1084.

20. Shami, A.-M.M.; Philip, K.; Muniandy, S. Synergy of antibacterial and antioxidant activities from crude extracts and peptides of selected plant mixture. *BMC Complement. Altern. Med.* **2013**, *13*, 360.

21. Williams, D.J.; Edwards, D.; Pun, S.; Chaliha, M.; Burren, B.; Tinggi, U.; Sultanbawa, Y. Organic acids in Kakadu plum (*Terminalia ferdinandiana*): The good (ellagic), the bad (oxalic) and the uncertain (ascorbic). *Food Res. Int.* **2016**, *89*, 237–244.

22. Williams, D.J.; Edwards, D.; Pun, S.; Chaliha, M.; Sultanbawa, Y. Profiling ellagic acid content: The importance of form and ascorbic acid levels. *Food Res. Int.* **2014**, *66*, 100–106.

23. Shalom, J.; Cock, I.E. *Terminalia ferdinandiana* Exell. fruit and leaf extracts inhibit proliferation and induce apoptosis in selected human cancer cell lines. *Nutr. Cancer* **2018**, *70*, 579–593.

24. Akter, R.; Kwak, G.-Y.; Ahn, J.C.; Mathiyalagan, R.; Ramadhania, Z.M.; Yang, D.C.; Kang, S.C. Protective Effect and Potential Antioxidant Role of Kakadu Plum Extracts on Alcohol-Induced Oxidative Damage in HepG2 Cells. *Appl. Sci.* **2022**, *12*, 236.

25. Nagajyothi, P.; Cha, S.J.; Yang, I.J.; Sreekanth, T.; Kim, K.J.; Shin, H.M. Antioxidant and anti-inflammatory activities of zinc oxide nanoparticles synthesized using *Polygala tenuifolia* root extract. *J. Photochem. Photobiol. B Biol.* **2015**, *146*, 10–17.

26. Abdelmigid, H.M.; Hussien, N.A.; Alyamani, A.A.; Morsi, M.M.; AlSufyani, N.M. Green Synthesis of Zinc Oxide Nanoparticles Using Pomegranate Fruit Peel and Solid Coffee Grounds vs. Chemical Method of Synthesis, with Their Biocompatibility and Antibacterial Properties Investigation. *Molecules* **2022**, *27*, 1236.

27. Basnet, P.; Chanu, T.I.; Samanta, D.; Chatterjee, S. A review on bio-synthesized zinc oxide nanoparticles using plant extracts as reductants and stabilizing agents. *J. Photochem. Photobiol. B Biol.* **2018**, *183*, 201–221.

28. El-Seedi, H.R.; El-Shabasy, R.M.; Khalifa, S.A.; Saeed, A.; Shah, A.; Shah, R.; Iftikhar, F.J.; Abdel-Daim, M.M.; Omri, A.; Hajrahand, N.H. Metal nanoparticles fabricated by green chemistry using natural extracts: Biosynthesis, mechanisms, and applications. *RSC Adv.* **2019**, *9*, 24539–24559.

29. Sharma, J.; Al-Omran, A.; Parvathy, S. Role of nitric oxide in inflammatory diseases. *Inflammopharmacology* **2007**, *15*, 252–259.

30. Salahuddin, N.A.; El-Kemary, M.; Ibrahim, E.M. Synthesis and characterization of ZnO nanoparticles via precipitation method: Effect of annealing temperature on particle size. *Nanosci. Nanotechnol.* **2015**, *5*, 82–88.

31. Akter, S.; Netzel, M.E.; Tinggi, U.; Osborne, S.A.; Fletcher, M.T.; Sultanbawa, Y. Antioxidant rich extracts of *Terminalia ferdinandiana* inhibit the growth of foodborne bacteria. *Foods* **2019**, *8*, 281.

32. Das, G.; Kim, D.-Y.; Fan, C.; Gutiérrez-Grijalva, E.P.; Heredia, J.B.; Nissapatorn, V.; Mitsuwan, W.; Pereira, M.L.; Nawaz, M.; Siyadatpanah, A. Plants of the genus *Terminalia*: An insight on its biological potentials, pre-clinical and clinical studies. *Front. Pharmacol.* **2020**, *11*, 6–11.

33. Aleixandre-Tudo, J.L.; Du Toit, W. The role of UV-visible spectroscopy for phenolic compounds quantification in winemaking. *Front. New Trends Sci. Ferment. Food Beverages* **2018**, *5*, 1–21.

34. Marslin, G.; Siram, K.; Maqbool, Q.; Selvakesavan, R.K.; Kruszka, D.; Kachlicki, P.; Franklin, G. Secondary metabolites in the green synthesis of metallic nanoparticles. *Materials* **2018**, *11*, 940.

35. Hoon Seo, K.; Markus, J.; Soshnikova, V.; Oh, K.H.; Anandapadmanaban, G.; Elizabeth Jimenez Perez, Z.; Mathiyalagan, R.; Kim, Y.J.; Yang, D.C. Facile and green synthesis of zinc oxide particles by *Stevia Rebaudiana* and its in vitro photocatalytic activity. *Inorg. Nano-Met. Chem.* **2019**, *49*, 1–6.

36. Wahab, R.; Ansari, S.; Kim, Y.; Seo, H.; Kim, G.; Khang, G.; Shin, H.-S. Low temperature solution synthesis and characterization of ZnO nano-flowers. *Mater. Res. Bull.* **2007**, *42*, 1640–1648.

37. Jayachandran, A.; Aswathy, T.; Nair, A.S. Green synthesis and characterization of zinc oxide nanoparticles using *Cayratia pedata* leaf extract. *Biochem. Biophys. Rep.* **2021**, *26*, 100995.

38. Muhammad, W.; Ullah, N.; Haroon, M.; Abbasi, B.H. Optical, morphological and biological analysis of zinc oxide nanoparticles (ZnO NPs) using *Papaver somniferum* L. *RSC Adv.* **2019**, *9*, 29541–29548.

39. Alamdari, S.; Sasani Ghamsari, M.; Lee, C.; Han, W.; Park, H.-H.; Tafreshi, M.J.; Afarideh, H.; Ara, M.H.M. Preparation and characterization of zinc oxide nanoparticles using leaf extract of *Sambucus ebulus*. *Appl. Sci.* **2020**, *10*, 3620.

40. Lanje, A.S.; Sharma, S.J.; Ningthoujam, R.S.; Ahn, J.-S.; Pode, R.B. Low temperature dielectric studies of zinc oxide (ZnO) nanoparticles prepared by precipitation method. *Adv. Powder Technol.* **2013**, *24*, 331–335.

41. Upadhyaya, L.; Singh, J.; Agarwal, V.; Pandey, A.; Verma, S.P.; Das, P.; Tewari, R. Efficient water soluble nanostructured ZnO grafted O-carboxymethyl chitosan/curcumin-nanocomposite for cancer therapy. *Process. Biochem.* **2015**, *50*, 678–688.

42. Saif, M.S.; Zafar, A.; Waqas, M.; Hassan, S.G.; ul Haq, A.; Tariq, T.; Batool, S.; Dilshad, M.; Hasan, M.; Shu, X. Phyto-reflexive Zinc Oxide Nano-Flowers synthesis: An advanced photocatalytic degradation and infectious therapy. *J. Mater. Res.* **2021**, *13*, 2375–2391.

43. Fakhari, S.; Jamzad, M.; Kabiri Fard, H. Green synthesis of zinc oxide nanoparticles: A comparison. *Green Chem. Lett. Rev.* **2019**, *12*, 19–24.

44. Goutam, S.P.; Yadav, A.K.; Das, A.J. Coriander extract mediated green synthesis of zinc oxide nanoparticles and their structural, optical and antibacterial properties. *J. Nanosci. Nanotechnol.* **2017**, *2*, 249–252.

45. Yedurkar, S.; Maurya, C.; Mahanwar, P. Biosynthesis of zinc oxide nanoparticles using *Ixora coccinea* leaf extract—A green approach. *OJSTA* **2016**, *5*, 1–14.

46. Kuruppu, K.; Perera, K.; Chamara, A.; Thiripuranathar, G. Flower shaped ZnO—NPs; phytofabrication, photocatalytic, fluorescence quenching, and photoluminescence activities. *Nano Express* **2020**, *1*, 20020.

47. Arefi, M.R.; Rezaei-Zarchi, S. Synthesis of zinc oxide nanoparticles and their effect on the compressive strength and setting time of self-compacted concrete paste as cementitious composites. *Int. J. Mol. Sci.* **2012**, *13*, 4340–4350.

48. Ramesh, M.; Anbuvannan, M.; Viruthagiri, G. Green synthesis of ZnO nanoparticles using *Solanum nigrum* leaf extract and their antibacterial activity. *Spectrochim. Acta Part. A Mol. Biomol. Spectrosc.* **2015**, *136*, 864–870.

49. Ahmad, Z.; Ullahkha, F.; Mahmood, S.; Mahmood, T.; Shamin, A. Different approaches for the synthesis of zinc oxide nanoparticles. *Open J. Chem* **2018**, *1*, 21–22.

50. Rajeshkumar, S.; Kumar, S.V.; Ramaiah, A.; Agarwal, H.; Lakshmi, T.; Roopan, S.M. Biosynthesis of zinc oxide nanoparticles using *Mangifera indica* leaves and evaluation of their antioxidant and cytotoxic properties in lung cancer (A549) cells. *Enzyme Microb. Technol.* **2018**, *117*, 91–95.

51. Darshita, M.; Sood, R. Review on synthesis and applications of zinc oxide nanoparticles. *Preprints* **2021,** *2021050688,* 12–13.

52. Ahmed, S.; Chaudhry, S.A.; Ikram, S. A review on biogenic synthesis of ZnO nanoparticles using plant extracts and microbes: A prospect towards green chemistry. *J. Photochem. Photobiol. B Biol.* **2017**, *166*, 272–284.

53. Mishra, P.K.; Mishra, H.; Ekielski, A.; Talegaonkar, S.; Vaidya, B. Zinc oxide nanoparticles: A promising nanomaterial for biomedical applications. *Drug Discov. Today* **2017**, *22*, 1825–1834.

54. Pandurangan, M.; Kim, D.H. In vitro toxicity of zinc oxide nanoparticles: A review. *J. Nanopart. Res.* **2015**, *17*, 1–8.

55. Liu, J.; Wang, Z. Increased oxidative stress as a selective anticancer therapy. *Oxid. Med. Cell. Longev.* **2015**, *1*, 4-6.

56. Tanino, R.; Amano, Y.; Tong, X.; Sun, R.; Tsubata, Y.; Harada, M.; Fujita, Y.; Isobe, T. Anticancer activity of ZnO nanoparticles against human small-cell lung cancer in an orthotopic mouse model. *Mol. Cancer Ther.* **2020**, *19*, 502–512.

57. Yi, C.; Yu, Z.; Ren, Q.; Liu, X.; Wang, Y.; Sun, X.; Yin, S.; Pan, J.; Huang, X. Nanoscale ZnO-based photosensitizers for photodynamic therapy. *Photodiagnosis Photodyn. Ther.* **2020**, *30*, 101694.

58. Kim, Y.J.; Perumalsamy, H.; Castro-Aceituno, V.; Kim, D.; Markus, J.; Lee, S.; Kim, S.; Liu, Y.; Yang, D.C. Photoluminescent and self-assembled hyaluronic acid-zinc oxide-ginsenoside Rh2 nanoparticles and their potential caspase-9 apoptotic mechanism towards cancer cell lines. *Int. J. Nanomed.* **2019**, *14*, 8195.

59. Dröse, S.; Brandt, U. Molecular mechanisms of superoxide production by the mitochondrial respiratory chain. *Adv. Exp. Med. Biol.* **2012**, *2*, 145–169.

60. Liu, B.; Chen, Y.; Clair, D.K.S. ROS and p53: A versatile partnership. *Free Radic. Biol. Med.* **2008**, *44*, 1529–1535.

61. Johnson, T.M.; Yu, Z.-X.; Ferrans, V.J.; Lowenstein, R.A.; Finkel, T. Reactive oxygen species are downstream mediators of p53-dependent apoptosis. *Proc. Natl. Acad. Sci. USA* **1996**, *93*, 11848–11852.

62. Aubrey, B.J.; Kelly, G.L.; Janic, A.; Herold, M.J.; Strasser, A. How does p53 induce apoptosis and how does this relate to p53-mediated tumour suppression? *Cell Death Differ.* **2018**, *25*, 104–113.

63. Chang, S.N.; Khan, I.; Kim, C.G.; Park, S.M.; Choi, D.K.; Lee, H.; Hwang, B.S.; Kang, S.C.; Park, J.G. Decursinol angelate arrest melanoma cell proliferation by initiating cell death and tumor shrinkage via induction of apoptosis. *Int. J. Mol. Sci.* **2021**, *22*, 4096.

64. Ghobrial, I.M.; Witzig, T.E.; Adjei, A.A. Targeting apoptosis pathways in cancer therapy. *CA Cancer J. Clin.* **2005**, *55*, 178–194.

65. Kim, Y.J.; Park, W. Anti-inflammatory effect of quercetin on RAW 264.7 mouse macrophages induced with polyinosinic-polycytidylic acid. *Molecules* **2016**, *21*, 450.